

QCD Studies at HERA*

Selected Topics

J. OLSSON

(on behalf of the H1 and ZEUS collaborations)

DESY, Notkestraße 85, 22603 Hamburg, Germany

E-mail: jan.olsson @ desy.de

Abstract

Several topics from the wide field of QCD studies in Deep-inelastic ep Scattering at HERA are addressed. They include QCD analyses of the inclusive cross section with the determination of α_s and the proton gluon density from the F_2 scaling violations, and the determination of the longitudinal structure function F_L . QCD analyses of inclusive jet and dijet data are also presented. Finally jet substructure and three-jet production are discussed.

1 Introduction

Studies of Deep-inelastic lepton-nucleon scattering (DIS) have played a fundamental role in establishing QCD as the strong interaction theory and in exploring the parton structure of the nucleon. With the advent of HERA, in which electrons or positrons of 27.5 GeV energy collide with protons of 820 GeV (in the last years 920 GeV), the tests of QCD have been extended by several orders of magnitude with respect to the range in Bjorken- x and in Q^2 , the squared momentum transfer between lepton and nucleon. The early fixed target experiments observed scaling violations, i.e. the variation of the structure functions with Q^2 . The scaling violations are well described by QCD, in which they are related to the gluon density in the proton, and to the strong interaction coupling constant, α_s .

At HERA the low x region was experimentally explored for the first time, and the first measurements[1] of the proton structure function $F_2(x, Q^2)$ revealed a steep rise of F_2 towards low x values, indicating a high gluon density in the proton at low x . A key question is then the validity of the DGLAP evolution equations[2] at low x values, since in the DGLAP evolution higher order terms proportional to $\alpha_s \cdot \ln(1/x)$ are neglected. One expects that at some value of x non-linear gluon interaction effects will become important, damping the

*Talk given at the Intern. Conference on New Trends in High Energy Physics, 22-29.9.2001, Yalta, Crimea, Ukraine.

rise of the cross section in accordance with unitarity requirements. While this question cannot yet be answered, the low x region remains a key area for future QCD studies at HERA.

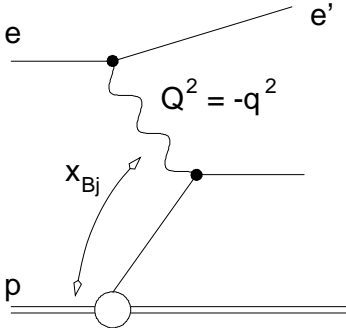


Figure 1: Diagram for lowest order ep DIS

At the same time as precision measurements of the inclusive DIS cross section and the proton structure functions are being pursued, QCD tests of processes of higher order in α_s are also being investigated. These tests involve the study of jet production in DIS, a field for which HERA is well suited with its large ep CMS energy $\sqrt{s} = 300\text{--}320$ GeV. This experimental work is intimately connected with theory development, since tests of higher order jet production need the corresponding processes to be quantitatively estimated.

2 The Inclusive DIS Cross Section and the Proton Structure

Inclusive ep neutral current (NC) DIS is to lowest order, $\mathcal{O}(\alpha_s^0)$, described by the diagram in Fig. 1, in which a virtual boson is emitted by the electron and scatters off a parton in the proton. In the one-photon exchange approximation, the double differential cross section can be written as

$$\frac{d^2\sigma}{dx dQ^2} = \frac{2\pi\alpha^2}{xQ^4} (Y_+ F_2(x, Q^2) - y^2 F_L(x, Q^2)), \quad Y_+ = 1 + (1 - y)^2.$$

The inelasticity $y = Q^2/xs$ represents the energy fraction transferred to the proton in the scattering process. F_2 and F_L are the (unpolarized, electromagnetic) proton structure functions and contain the information about the momentum distribution of partons in the proton. They are not calculable in theory and have to be measured. However, when measured at a given Q^2 value, their evolution in Q^2 can be predicted in theory.

The NC DIS cross section can also be written as

$$\frac{d^2\sigma}{dx dQ^2} = \Gamma(y) (\sigma_T + \epsilon(y) \sigma_L)$$

where the ep scattering process is considered as the interaction of a flux of virtual photons with the proton. Here $\Gamma(y) = Y_+ \alpha / (2\pi Q^2 x)$ is the flux factor and $\epsilon(y) = 2(1 - y)/Y_+$ defines the photon polarization. σ_T and σ_L are the cross sections of the interaction of transverse and longitudinally polarized photons with the proton. These cross sections are related to the structure functions:

$$F_2(x, Q^2) = \frac{Q^2}{4\pi^2\alpha} (\sigma_T(x, Q^2) + \sigma_L(x, Q^2)) \quad \text{and} \quad F_L(x, Q^2) = \frac{Q^2}{4\pi^2\alpha} \sigma_L(x, Q^2).$$

Due to cross section positivity, the relation $0 \leq F_L \leq F_2$ is obeyed.

In the QPM world, without gluons, $\sigma_L = 0$, since longitudinally polarized photons do not interact with massless spin 1/2 partons. Thus, in QPM also $F_L = 0$ [3]. In QCD quarks radiate gluons and interact through gluon exchange. Radiated gluons in turn can split into quark-antiquark pairs (“sea quarks”) or gluons. The gluon radiation results in a transverse momentum component of the quarks, which can now also couple to longitudinally polarized photons.

Thus, σ_L and F_L get non-zero values. Due to its origin, F_L is directly dependent on the gluon distribution in the proton and therefore the measurement of F_L provides a sensitive test of QCD at low x values. In fact, the low x region cannot be understood without measuring F_L precisely.

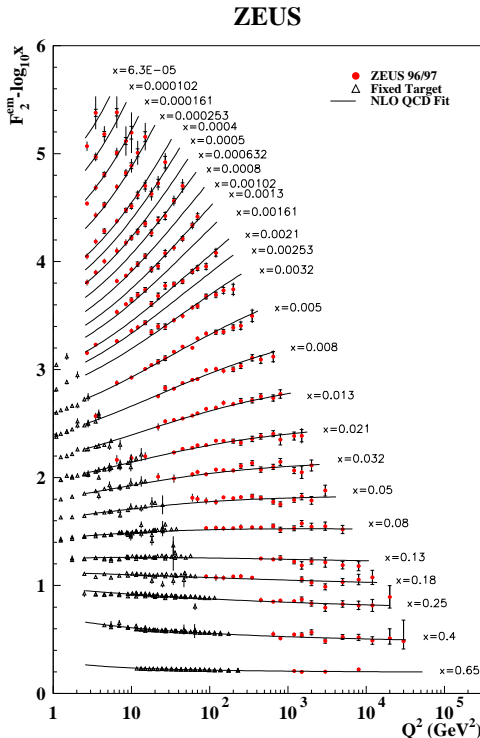


Figure 2: F_2 vs Q^2 , for fixed values of x . Data from ZEUS and fixed target experiments. The curves show the NLO QCD fit to the data.

The ep cross section is usually written in the “reduced” form, in which the Q^2 dependence due to the photon propagator is removed,

$$\sigma_r \equiv F_2(x, Q^2) - \frac{y^2}{Y_+} F_L(x, Q^2).$$

Since the contribution of the longitudinal structure function F_L to the cross section can be sizeable only at large values of y , in a large kinematic range the relation $\sigma_r \approx F_2$ holds to a very good approximation.

The H1 and ZEUS collaborations have recently presented high statistics measurements[4, 5, 6] of the NC DIS cross section and extracted F_2 in the kinematic range $1.5 - 2.7 < Q^2 < 30000 \text{ GeV}^2$ and $3 - 6 \cdot 10^{-5} < x < 0.65$. The ZEUS data are shown in Fig. 2. The strong (positive) scaling violations at low x values, due to the increase of the gluon density ($\frac{\partial F_2}{\partial \log Q^2} \sim \alpha_s x g$ at low x), are clearly seen. At large x values negative scaling violations appear ($\frac{\partial F_2}{\partial \log Q^2} \sim \alpha_s F_2$ at large x).

The ZEUS and H1 data are in very good agreement, both with each other and, at the largest x values where data overlap, with the earlier fixed target experiments.

Both collaborations have subjected their F_2 data to extensive QCD analyses in next-to-leading-order (NLO), extracting the parton density functions (PDFs) and α_s [5, 7]. While the general analysis and fit strategy is similar in both collaborations, there are also many differences in the details, e.g. in the density parametrizations and in the treatment of flavour number and in the use of the fixed target data. An extensive discussion can be found in [8].

Fig. 2 shows that the NLO QCD fits, which are based on the DGLAP evolution, describe the data very well over no less than four orders of magnitude and down to surprisingly low Q^2 of a few GeV^2 . The gluon density extracted in the NLO QCD fits is shown for both experiments in Fig. 3 for three values of Q^2 . Within the error bands there is reasonable agreement. Like F_2 , the gluon density increases towards low x values, and the increase is steeper with increasing Q^2 .

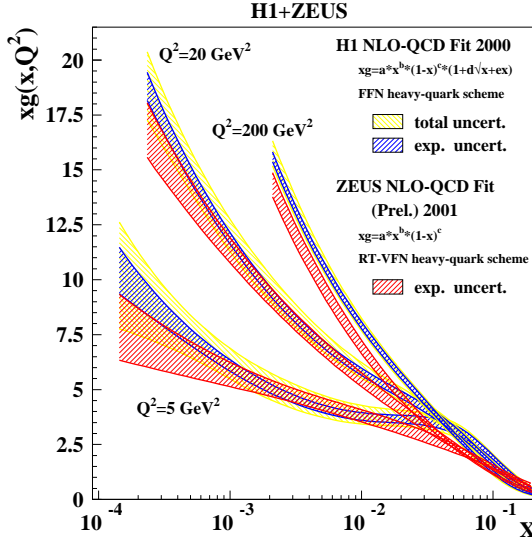


Figure 3: Gluon density for three different values of Q^2 . The error bands show the experimental and (for H1) also the total (including theoretical) uncertainty.

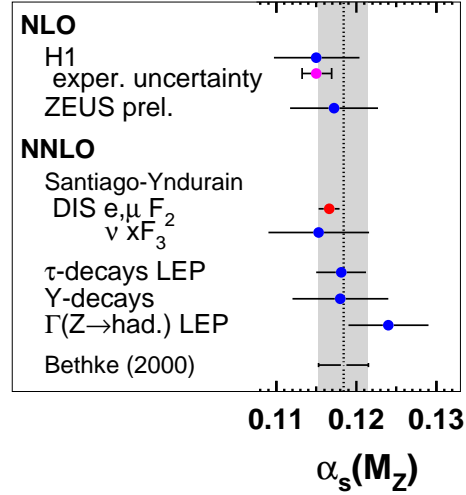


Figure 4: α_s values obtained in the NLO QCD analyses of F_2 data. Also shown are α_s values obtained in a recent NNLO analysis[10] as well as other α_s values obtained at NNLO level.

The α_s values obtained in the NLO fits of H1 and ZEUS are shown in Fig. 4¹. In the H1 case also the error due only to the experimental uncertainty is shown. Thus, the theoretical uncertainty dominates the total error. The major part of this error is due to the choice of renormalization scale, and to a lesser extent, also to the choice of the factorization scale. This is expected to change once next-to-next-to-leading-order (NNLO) QCD calculations are available. Fig. 4 also shows the result of a recent NNLO analysis of ep DIS data[10], in which the moments of F_2 are fitted to obtain an impressingly small error on α_s . Comparing the ep DIS α_s result with the result obtained when using the more imprecise νN scattering data, or with the α_s values obtained in NNLO for τ -decays, Y -decays, or in analysis of $\Gamma(Z)$, it is obvious that the ep DIS data are very competitive in precision determinations of α_s . Note that the analysis in [10] used earlier data on F_2 [11], and not yet the most recent, very precise data.

Both collaborations are working on further reduction of the experimental errors on the F_2 data, errors which are completely dominated by systematics, in particular the uncertainty on the calorimetric energy scale. Clearly, theoretical progress is essential in order to profit from future, still better experimental precision in the F_2 data.

3 The Longitudinal Structure Function F_L

A fully independent measurement of F_L at HERA, in a wide range of x and Q^2 , is only possible via a substantial variation of the beam energies; at any

¹Figure courtesy M. Erdmann, LP2001, Rome 2001[9].

given values of x and Q^2 the difference of the reduced cross section, measured at two values of the CMS energy $s = Q^2/xy$, is a direct measure of F_L :

$$\sigma_{r,1} - \sigma_{r,2} = [(y^2/Y_+)_1 - (y^2/Y_+)_2] \cdot F_L.$$

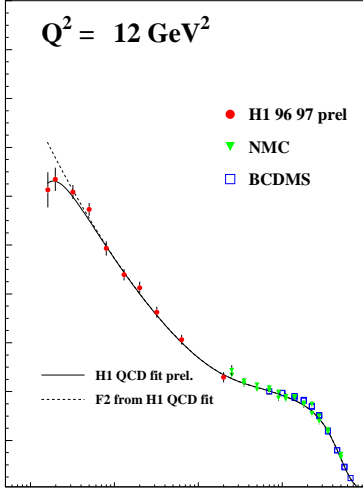


Figure 5: Reduced cross section vs. x , for $Q^2 = 12 \text{ GeV}^2$. The curves are due to the H1 NLO QCD fit and represent F_2 and the cross section.

This measurement is not yet performed but is part of the HERA II physics program[12]. While waiting for this to happen, the H1 collaboration has performed several indirect extractions of F_L . The methods of extraction are based on the direct measurement of the cross section in the high y region, and on the extrapolation of the precise knowledge of F_2 at low values of y , into the region of high y . Cross section measurements of the NC DIS process in the high y region pose a challenge to the HERA experiments, since low energy (down to 3 GeV is achieved) scattered electrons have to be triggered, identified and well measured. The detailed understanding of the detector and of the photoproduction background is essential and an important part of the measurement is therefore the improvement of both calorimetry and the detection of charged tracks in the H1 central and backward regions. The measurement of track charge and momentum at all scattering angles is particularly important in

estimating the amount and shape of the background from photon conversions (with photons from the $\pi^0 \rightarrow \gamma\gamma$ decay), through the identification of "wrong" charge electrons.

Two methods are used for the extraction of F_L from the cross section measurements, namely the "subtraction" method applied at $Q^2 > 10 \text{ GeV}^2$, and the "derivative" method, applied for $Q^2 < 10 \text{ GeV}^2$. The subtraction method is illustrated in Fig. 5, showing the reduced cross section as function of x at fixed $Q^2 = 12 \text{ GeV}^2$. At the lowest x values (corresponding to high y values) the cross section falls below the F_2 curve, extrapolated via the H1 NLO QCD fit. Thus, F_L is obtained from the difference $F_2 - \sigma_r$. This method was first explored in [13] and in the recent analyses, using data from 1996-97[5] and 1998-2000[14], F_L is extracted up to Q^2 values of 700 GeV^2 . Fig. 6 shows the Q^2 dependence of F_L , separately for e^+p and e^-p data. As it should be, F_L is independent of the lepton beam. One also sees that F_L is clearly different from the extreme possibilities, $F_L = 0$ or $F_L = F_2$. Within the present precision of the data there is good agreement with the QCD expectation, as projected using the H1 NLO fit.

In the second method of extracting F_L , the derivative of the reduced cross section with respect to $\ln y$ is formed:

$$\left(\frac{\partial \sigma_r}{\partial \ln y} \right)_{Q^2} = \left(\frac{\partial F_2}{\partial \ln y} \right)_{Q^2} - F_L \cdot 2y^2 \cdot \frac{2-y}{Y_+^2} - \frac{\partial F_L}{\partial \ln y} \cdot \frac{y^2}{Y_+}.$$

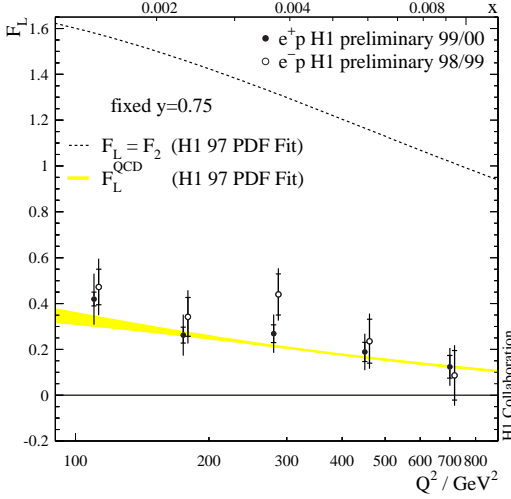


Figure 6: F_L vs. Q^2 (or, equivalently, vs. x , upper scale), for fixed $y = 0.75$, for e^+p and e^-p data. The curves show the H1 NLO QCD fit, obtained for several assumptions on F_L . The shaded band shows the expectation for F_L and its uncertainty from the QCD fit.

For $y \rightarrow 1$ the cross section derivative tends to the limit $(\partial F_2 / \partial \ln y)_{Q^2} - 2 \cdot F_L$, neglecting the contribution from the derivative of F_L . At largest y the F_L contribution dominates the derivative of the reduced cross section σ_r . This is in contrast to the influence of F_L on σ_r which is dominated by the contribution of F_2 for all y . A further advantage of the derivative method is that it can be applied down to very low $Q^2 \simeq 1 \text{ GeV}^2$ where a QCD description of $F_2(x, Q^2)$ is complicated due to higher order and possible non-perturbative corrections. The measured cross section derivative is shown in Fig. 7 as a function of y , in several bins of Q^2 . Since for a given Q^2 value, $F_2 \sim x^{-\lambda} \sim e^{\lambda \ln y}$, and since λ is small for low values of Q^2 , $\frac{\partial F_2}{\partial \ln y}$ is linear in $\ln y$ to good approximation. This is clearly seen in Fig. 7. In each Q^2 bin straight line fits were made to the de-

rivative data for $y < 0.3$. The line fits describe the data very well and the extrapolation of the straight line was taken to represent the contribution of F_2 at high y . The small contribution of $\partial F_L / \partial \ln y$ to the derivative was corrected for by using NLO QCD and the correction was included in the overall error of the measured F_L . The derivative method was used in the analysis of the low Q^2 data, both in the 1996-97 data[5] and in the 1999-2000 data[14]. Since the latter data have higher p beam energy, 920 GeV as compared to 820 GeV in the earlier data, the accessible x range could be extended to even smaller values. It is also worthwhile to note that the H1 NLO fit is based on the 1996-97 data; when using this fit in the analyses of the later data proper account was taken in order to correct for the difference in p beam energy.

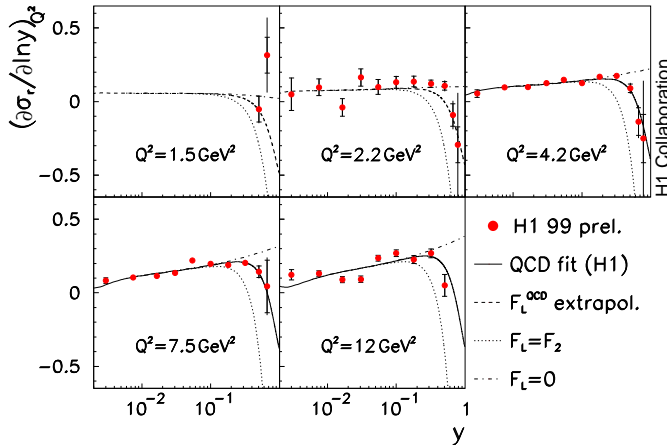


Figure 7: Measurement of $(\partial \sigma_r / \partial \ln y)_{Q^2}$ vs. y , in bins of Q^2 . The curves represent the NLO QCD fit to the H1 1996/97 data for $y < 0.35$ and $Q^2 \geq 3.5 \text{ GeV}^2$, calculated for several assumptions on F_L .

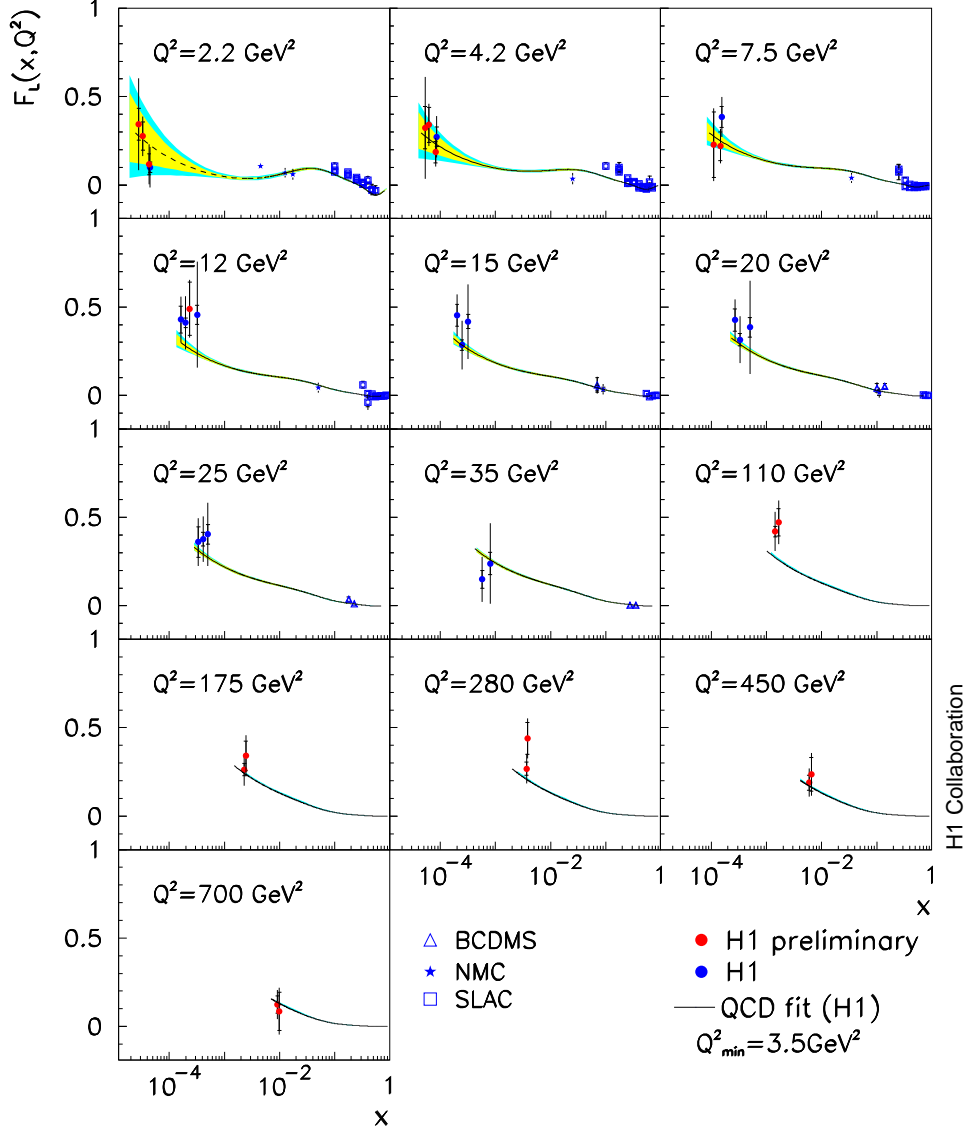


Figure 8: Longitudinal Structure Function F_L vs. x and in bins of Q^2 , obtained by H1 and fixed target experiments. Error bands are due to experimental (inner) and model (outer) uncertainties using the H1 NLO QCD fit to the H1 1996/97 data for $y < 0.35$ and $Q^2 \geq 3.5 \text{ GeV}^2$.

Fig. 8 gives an overview of the current H1 data on $F_L(x, Q^2)$ in the Q^2 range $2.2 - 700 \text{ GeV}^2$ [5, 14]. The data extend the knowledge of F_L into the region of low x , much beyond the range of the fixed target experiments. The increase of $F_L(x, Q^2)$ towards low x is consistent with the NLO QCD calculation, reflecting the rise of the gluon density in this region. The values of $F_L(x, Q^2)$ are thus severely constrained by the present data, unless there are deviations from the assumed extrapolation of F_2 into the region of large y corresponding to the smallest x .

F_L has also been calculated in the ZEUS NLO QCD fit[7]; the calculation is consistent with the H1 data.

4 Inclusive Jets and Dijets in DIS

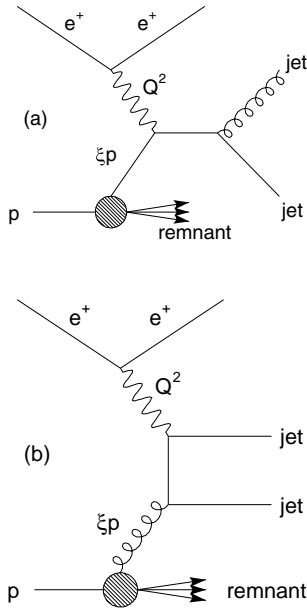


Figure 9: Diagrams for QCD Compton and Boson Gluon Fusion processes.

The fully inclusive DIS process, shown in Fig. 1, is of zero order in α_s . There is direct sensitivity only to the quark PDF's, and the determination of α_s and gluon density is indirect, via the scaling violations of F_2 , measured over a large range of x and Q^2 .

The DIS processes shown in Figs. 9a and b, QCD Compton (QCDC) scattering and Boson Gluon Fusion (BGF), are of order α_s and due to the latter contribution there is direct sensitivity to the gluon density of the proton. At high enough energy, the involved final state partons manifest as jets of hadrons. The multi-jet final state can be characterized by the jet mass, M_{jj} , and the variable $\xi = x_{Bj}(1 + M_{jj}^2/Q^2)$. The dijet mass M_{jj} gives the CM energy of the boson-parton reaction and the fractional momentum x (the longitudinal momentum fraction of the proton carried by the parton specified by the PDFs) is given by ξ , which is much larger than x_{Bj} if M_{jj} is large.

Two hard scales enter in these diagrams, Q^2 and $E_{T,jet}$. Studies of the dynamics of multi-jet production are usually performed in the Breit frame, where the virtual boson interacts head-on with the proton[15]. In lowest order, $\mathcal{O}(\alpha_s^0)$, the parton from

the proton is backscattered into opposite direction, and no transverse energy is produced. Thus, appearance of jets with large E_T can only be explained by hard QCD processes of at least $\mathcal{O}(\alpha_s)$, and $E_{T,jet}$ is then the physical scale at which e.g. hard gluon radiation is resolved. Experimentally, jets are usually identified using a k_T algorithm[16].

The H1 and ZEUS collaborations have recently presented high statistics studies of inclusive jet and dijet production in NC DIS[17, 18, 19, 20]. The data span the kinematic range $5 - 10 < Q^2 < 10 - 15 \cdot 10^3 \text{ GeV}^2$ and $5 - 7 < E_{T,jet} < 60 \text{ GeV}$. NLO QCD calculations in general describe the data very well, over almost the whole range of Q^2 and $E_{T,jet}$. This is exemplified in Fig. 10, showing the H1 inclusive jet cross section as function of $E_{T,jet}$ and Q^2 , and in Fig. 11, showing the ZEUS dijet cross section as function of Q^2 . The largest uncertainty in the QCD calculations stems from the uncertainty in the choice of renormalization scale μ_r , which is taken either as Q or as mean jet transverse energy, $\overline{E}_{T,jet}$. The uncertainty is largest for low Q^2 values (Fig. 11b), and cuts are made at 150 (H1) and 470 (ZEUS) GeV^2 in the QCD analyses of the data. At large values of Q^2 the experimental uncertainties are also smaller, and this is true as well for the hadronic (parton-to-hadron) corrections to the NLO calculations, as shown in Figs. 10 and 11c.

Once the good agreement of the QCD calculation with the jet data has been established, one can proceed to perform a QCD analysis, determining α_s and

the gluon density. The analysis strategy is as follows:

1. Fit the jet data to the NLO QCD predictions, using PDFs obtained from global, external fits[21, 22]. With the PDFs externally fixed, there is only one free parameter, namely α_s . Note that the PDFs themselves depend implicitly on α_s , and that this complication was properly taken into account in the fits.
2. After establishing that the fitted α_s value agrees well with other, external measurements, α_s is fixed (e.g. to the world average) and the jet data are then fitted in order to extract the PDFs, in particular the gluon density of the proton.
3. Finally, a global, simultaneous fit of both α_s and the PDFs can be performed. This would be a more independent test of QCD with the data. However, although in this global fit the quark PDFs emerge as identical to those resulting from the fit in step (2), the simultaneous fit fails to produce meaningful results for α_s and the gluon density. The reason is

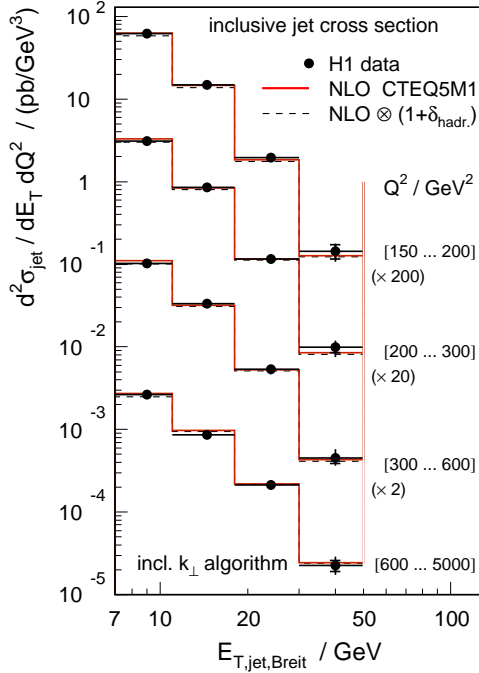


Figure 10: Inclusive jet cross section vs. $E_{T,jet}$, in several intervals of Q^2 . Also shown are NLO QCD calculations, with and without hadronic corrections.

the strong anti-correlation between α_s and the gluon density, which can be understood from the fact that in the phase space region considered, jet production is dominated by the gluon contribution, which enters in the cross section as the product $\alpha_s \cdot xg(x)$.

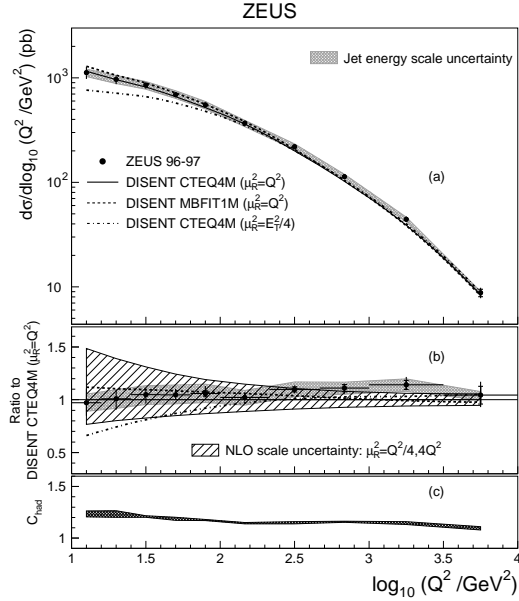


Figure 11: Dijet cross section vs. Q^2 . The shaded band represents the calorimeter energy scale uncertainty. The curves show NLO QCD calculations for several choices of μ_r and proton PDF sets. b) Ratio data/theory showing in addition the effect of the theoretical scale uncertainty. c) Parton-to-hadron correction.

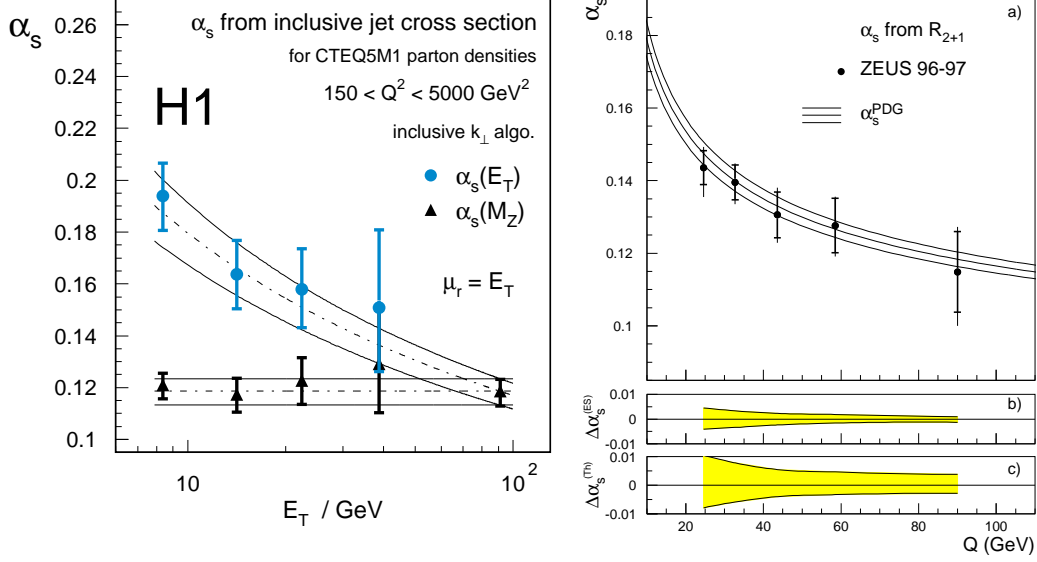


Figure 12: α_s running in 2 scales, $E_{T,jet}$ and Q . Uncertainties due to calorimeter energy scale and to theory are indicated in the ZEUS plot. Upper curves show the RGE prediction.

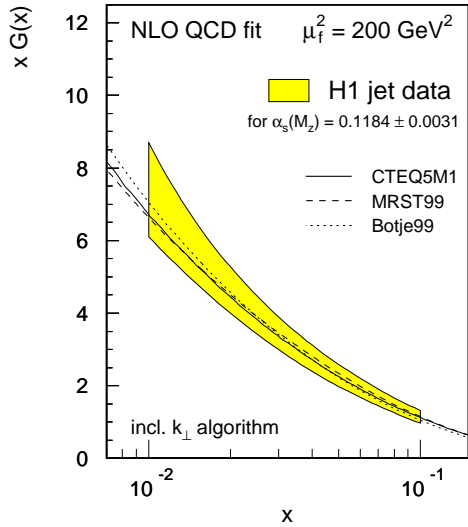


Figure 13: Gluon density in the proton, determined in a combined QCD fit using inclusive DIS, inclusive jet and dijet cross sections. The error band includes all experimental and theoretical uncertainties, also that of $\alpha_s(M_Z)$.

Both H1 and ZEUS have performed step 1 in this strategy, and the resulting α_s measurements are shown in Fig. 11. Note that the “running” of α_s is here clearly seen in both scales, Q and $E_{T,jet}$, and the running is moreover seen within each single experiment. The running is consistent with the renormalization group equation (RGE). The comparison of the measurements with other HERA measurements, and with the world average values is given in Fig. 15. The fact that the α_s values obtained from the DIS jet data agree very well with other measurements, in particular with measurements from processes which do not involve hadrons in the initial state, like e^+e^- annihilation to hadrons, can be taken as proof of the validity of perturbative QCD at NLO in DIS jet production.

Step 2 in the strategy was performed by H1, and the gluon density extracted from the data is shown in Fig. 13. The fit includes the combined cross sections of inclusive jet data, dijet data and inclusive DIS. The result is in good agreement with recent global analyses[21, 22, 23]. For a detailed comparison of this result with the gluon densities obtained from the F_2 scaling violations, see [24].

5 Jet Substructure

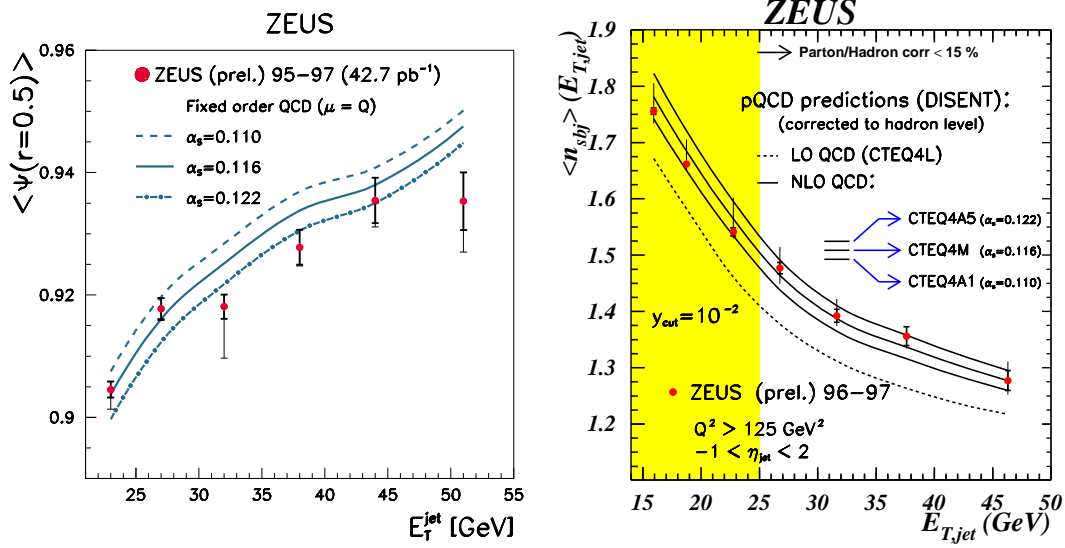


Figure 14: a) Integrated jet shape and b) mean subjet multiplicity as functions of $E_{T,jet}$. NLO QCD calculations are shown for three different values of α_s .

At sufficiently high transverse jet energy, $E_{T,jet}$ (or E_T^{jet}), fragmentation effects become negligible and both the shape and other features of the internal jet structure are expected to be calculable in perturbative QCD. The ZEUS collaboration has recently presented[25] several results based on studies of jet substructure, using the variables[26, 27] “integrated jet shape” $\Psi(r)$ and “mean subjet multiplicity” $\langle n_{subjet} \rangle$:

$$\Psi(r) = \frac{1}{N_{jet}} \sum_1^{N_{jet}} \frac{E_T^{jet}(r)}{E_T^{jet}(r=R)} \quad \text{and} \quad \langle n_{subjet} \rangle = \frac{1}{N_{jet}} \sum_1^{N_{jet}} n_{subjet}.$$

The radius r is defined in $\phi - \eta$ space, where the jet search is performed. The subjets within a given jet are found by repeating the jet algorithm with smaller resolution scale.

Among the results presented in [25] are

- The average subjet multiplicity in jets in Charged Current (CC) and NC events is found to be similar. Since the jets in CC and NC DIS are predominatly quark initiated, the similarity in jet substructure indicates that the pattern of parton radiation within a quark jet is independent of the specific hard scattering process.
- In a dijet event sample, c -quark jets were tagged through the identification of a D^* meson. The internal structure of the charm induced jets is found to be similar to that of the quark jets in NC DIS. Since the latter are dominantly light quark initiated, one can conclude that the evolution of the outgoing partons, which determines the internal structure of the jet, is independent of the hard subprocess from which the outgoing partons originate.

- Using the internal jet structure of the tagged, charm induced jets in the dijet event sample, and comparing with the internal jet structure of the total dijet sample, it was possible to extract the internal jet structure of gluon jets. The prediction of QCD, that gluon jets are broader, and contain more subjets, is nicely confirmed.

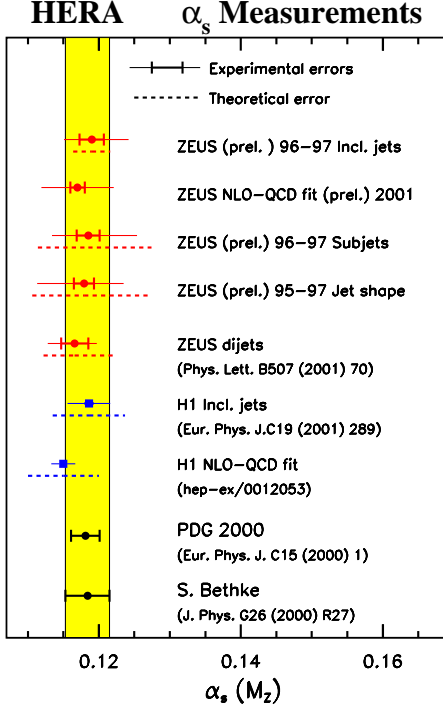


Figure 15: Summary of α_s measurements at HERA (given at the Z mass), using inclusive DIS data and NLO QCD fits, inclusive jets and dijets, and jet shape and subjet multiplicity. Also shown are the world average values (PDG 2000, S. Bethke).

The internal jet structure is sensitive to α_s beyond leading order. This sensitivity is demonstrated in Fig. 14 a and b, where the integrated jet shape (for $r = 0.5$) and mean subjet multiplicity is shown as functions of $E_{T,jet}$. Note that the jets become narrower, and that the mean subjet multiplicity decreases as $E_{T,jet}$ increases. The NLO QCD calculation describes both jetshape and mean subjet multiplicity well, but the calculation also varies strongly with different values of α_s . It is thus clear that the jet substructure data can be used to determine α_s . The method is similar to the one used in the QCD analysis of the inclusive and dijet data described above. External sets of PDFs are used, and the implicit dependence on α_s in these sets is properly taken account of in the fitting.

The results of the α_s determination using the jet substructure are shown in Fig. 15, together with other α_s measurements from HERA. These new measurements agree well with the others, which is proof of the consistency of the NLO QCD calculations also where the internal jet structure is concerned.

A general remark about the measurements in Fig. 15 can be made: The experimental errors in these measurements are small and comparable to the error on the world averages[28, 29]. The total errors on the α_s measurements at HERA are in fact everywhere dominated by the theoretical uncertainty. As already noted above, this situation is expected to change when NNLO calculations become available.

The Three-Jet Final State in DIS

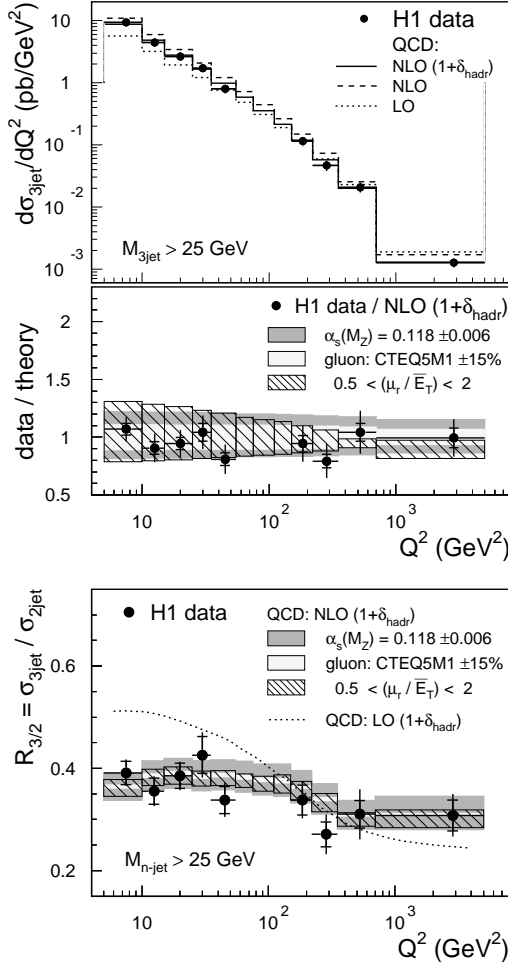


Figure 16: a) Inclusive three-jet cross section vs. Q^2 . Also shown is the ratio of data to theoretical prediction. b) Ratio of inclusive three-jet and dijet cross sections vs. Q^2 . LO and NLO QCD calculations are also shown, including the effects of variation in the latter of $\alpha_s(M_Z)$, renormalization scale μ_r and proton gluon density.

While the inclusive jet and dijet cross sections are directly sensitive to QCD effects of order $\mathcal{O}(\alpha_s)$, the three-jet cross section in DIS is already proportional to α_s^2 in leading order in perturbative QCD. This higher sensitivity to α_s and the greater number of degrees of freedom of the three-jet final state allow the QCD predictions to be tested in more detail in three-jet production. The H1 collaboration has recently presented[30] a study of DIS three-jet events, covering the kinematic range $5 < Q^2 < 5000$ GeV² and three-jet masses $25 < M_{3jet} < 140$ GeV. The Q^2 dependence of the cross section is shown in Fig. 16a, together with QCD LO and NLO calculations, the latter with and without hadronic corrections. The NLO calculation, which is due to the recently available program NLOJET[31], describes the data well over the whole kinematic range, as is also seen in the ratio of data to theory. In the latter plot are also shown the theory uncertainty due to variation of the gluon density, the renormalization scale $\mu_r = \bar{E}_T$ and α_s . As seen, at large $Q^2 > 50$ GeV² the α_s variation gives the largest uncertainty.

Since both dijet and three-jet production is dominated by gluon induced processes, the uncertainty of the gluon density can be minimized by taking the ratio $R_{3/2}$ of three-jet

and dijet cross sections, at the same values of x and M_{n-jet} . It can be shown, using the QCD calculations, that dijet and three-jet production involves the same gluon fraction, at similar Q^2 values. Furthermore, many experimental and systematic errors cancel in the ratio. As is evident in Fig. 16b, $R_{3/2}$, which is directly proportional to α_s , is experimentally measured and theoretically calculated with small uncertainties over the whole Q^2 range. Thus, given better statistics, a very sensitive test of QCD will be possible with the three-jet data, including a precision measurement of α_s .

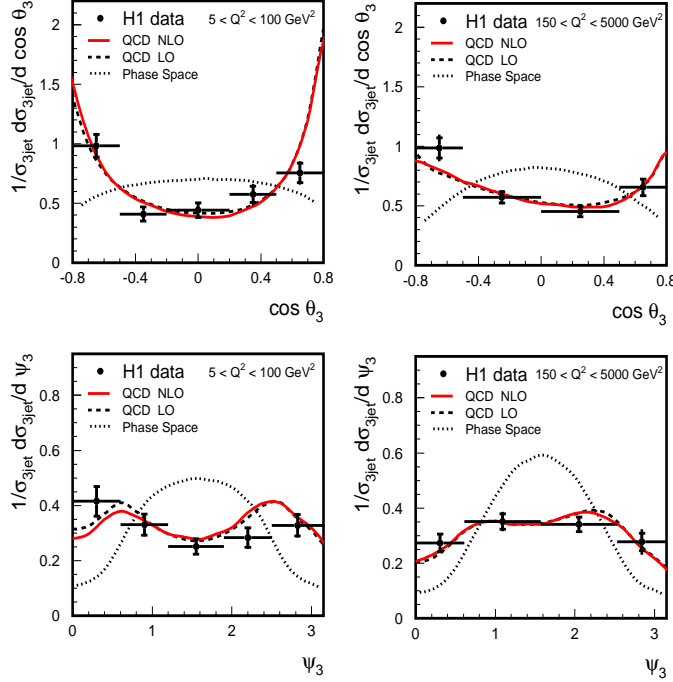


Figure 17: Normalized distributions of $\cos \theta_3$ and angle ψ_3 in the three-jet CMS at low Q^2 and high Q^2 . Solid and dashed curves show NLO and LO QCD calculations, dotted curves show a three-jet phase space model.

The topology of the three-jet final state offers a test of QCD through the angular distributions of θ_3 and ψ_3 , where θ_3 is the angle between the highest energy jet and the proton beam, and ψ_3 is the angle between the two planes formed by the highest energy jet and the proton beam, and by the three jets, respectively. These angles are shown in Fig. 17, for two Q^2 ranges. Both LO and NLO QCD calculations describe these normalized distributions well, while a phase space model fails the description. The distributions show that the jets tend to be aligned with either the photon or

the proton, i.e. the Bremsstrahlung nature of the process (coherence property of QCD) is confirmed. Similar distributions were previously also observed by the ZEUS collaboration in three-jet photoproduction[32].

Conclusions

The DIS data are well described by NLO QCD and the DGLAP evolution, over a large range of Q^2 and Bjorken- x . This is true for the inclusive DIS cross section, with the structure functions F_2 and F_L , as well as for the inclusive jet production and the exclusive dijet and three-jet production and for the internal structure of jets.

In many areas the data have reached a high experimental precision, and progress in the tests of perturbative QCD depends crucially on further progress in the theory, where the NNLO calculations for the DIS processes are awaited. This is particularly true for the precision determination of α_s at HERA, using DIS data, where the experimental precision is already at level with the error on the world average, and is expected to improve even further.

The running of α_s in accordance with the RGE is seen within each single experiment, and in both hard scales, Q and $E_{T,jet}$.

Some areas, like jets at highest Q^2 and $E_{T,jet}$, and the three-jet final state, are still statistically limited. The HERA II running period will bring a huge improvement of statistics in the coming years. However, in the analyses de-

scribed in this report, the experiments have in many cases so far only used the data taken in 1995-97, which constitute only about 1/3 of the total HERA I data. The remaining 2/3 of the HERA I data, from the years 1998-2000, is currently being recalibrated and reprocessed, and will soon be available.

Acknowledgments

It is a pleasure to thank the organizers for the warm and joyful atmosphere in a most interesting and remarkably well prepared conference. I also wish to thank my colleagues in H1 and ZEUS, for providing the data and results presented in this report and for all their help given to me.

References

- [1] H1 Collaboration, I. Abt et al., Nucl.Phys. **B407** (1993) 515;
ZEUS Collaboration, M. Derrick et al., Phys.Lett. **B316** (1993) 412.
- [2] L.V. Gribov and L.N. Lipatov, Sov.J.Nucl.Phys. **15**, (1972) 438 and 675;
L.N. Lipatov, Yad.Fiz **20** (1974) 181;
Yu.L. Dokshitzer, Sov. Phys. JETP **46** (1977) 641;
G. Altarelli and G. Parisi, Nucl.Phys. **B126** (1977) 298.
- [3] C.G. Callan and D.J. Gross, Phys.Rev.Lett. **22** (1969) 156.
- [4] H1 Collaboration, C. Adloff et al., Eur.Phys.J. **C13** (2000) 609.
- [5] H1 Collaboration, C. Adloff et al., Eur.Phys.J. **C21** (2001) 33.
- [6] ZEUS Collaboration, S. Chekanov et al., Eur.Phys.J. **C21** (2001) 443.
- [7] ZEUS Collaboration, Paper no. 628 submitted to the International Europhysics Conference on High Energy Physics, EPS2001, July, 2001, Budapest.
- [8] K. Nagano, in proceedings “New Trends in HERA Physics 2001”, Ringberg Workshop 17-22.6.2001.
- [9] M. Erdmann, hep-ex/0111052.
- [10] J. Santiago, F.J. Ynduráin, Nucl.Phys. **B611** (2001) 447.
- [11] H1 Collaboration, S. Aid et al., Nucl.Phys. **B470** (1996) 3;
ZEUS Collaboration, M. Derrick et al., Z.Phys. **C72** (1996) 399.
- [12] L. Bauerdick, A. Glazov, M. Klein, Future Measurement of the Longitudinal Proton Structure Function at HERA, Proc. Workshop on Future Physics at HERA, eds. G. Ingelmann, A. De Roeck, R. Klanner, Hamburg, DESY (1996), p.77; hep-ex/9609017 (1996).
- [13] H1 Collaboration, S. Aid et al., Phys.Lett. **B393** (1997) 452.
- [14] H1 Collaboration, Papers no. 787 and 799 submitted to the International Europhysics Conference on High Energy Physics, EPS2001, July, 2001, Budapest.
- [15] B.R. Webber, J.Phys. **G19** (1993) 1567.
- [16] S.D. Ellis and D.E. Soper, Phys.Rev. **D48** (1993) 3160;
S. Catani et al., Nucl.Phys. **B406** (1993) 187.
- [17] H1 Collaboration, C. Adloff et al., Eur.Phys.J. **C19** (2001) 289.

- [18] ZEUS Collaboration, Paper no. 637 submitted to the International Europhysics Conference on High Energy Physics, EPS2001, July, 2001, Budapest.
- [19] ZEUS Collaboration, J. Breitweg et al., DESY Preprint 01-018 (2001).
- [20] ZEUS Collaboration, S. Chekanov et al., DESY Preprint 01-127 (2001).
- [21] H.I. Lai et al., Eur.Phys.J. **C12** (2000) 375.
- [22] M. Botje, Eur.Phys.J. **C14** (2000) 285.
- [23] A.D. Martin et al., Eur.Phys.J. **C14** (2000) 133.
- [24] H1 Collaboration, Paper no. 992 submitted to the International Conference on High Energy Physics, ICHEP2000, July, 2000, Osaka.
- [25] ZEUS Collaboration, Papers no. 640, 641 and 646 submitted to the International Europhysics Conference on High Energy Physics, EPS2001, July, 2001, Budapest.
- [26] S.D. Ellis, Z. Kunszt and D.E. Soper, Phys.Rev.Lett. **69** (1992) 3615.
- [27] S. Catani et al., Nucl.Phys. **B377** (1992) 445; *ibid.* **B383** (1992) 419;
M.H. Seymour, Nucl.Phys. **B421** (1994) 545;
M.H. Seymour, Phys.Lett. **B378** (1996) 279.
- [28] Particle Data Group Report, D.E. Groom et al., Eur.Phys.J. **C15** (2000) 1.
- [29] S. Bethke, J.Phys. **G26** (2000) R27.
- [30] H1 Collaboration, C. Adloff et al., Phys.Lett. **B515** (2001) 17.
- [31] Z. Nagy and Z. Trócsányi, hep-ph/0104315.
- [32] ZEUS Collaboration, J. Breitweg et al., Phys.Lett. **B443** (1998) 394.